FULL PAPER

Photovoltaic Mode Ultraviolet Organic Photodetectors with High On/Off Ratio and Fast Response

Hugh L. Zhu, Wallace C. H. Choy, Wei E. I. Sha, and Xingang Ren*

Ultraviolet (UV) organic photodetectors (OPDs) operated in the photovoltaic mode, achieving a very high on/off ratio of 10^5 and a fast response time of 20 ns (a decay time of 888 ns), are demonstrated in this work. Light-induced tuning of the barrier height at the two interfaces of the carrier-extraction layer and light-induced tuning of series resistance are proposed to obtain the high on/off ratio. Fast response of the device is demonstrated through the ultrafast trap filling process. The high on/off ratio and fast response are simultaneously realized by introducing TiO_2 nanocrystals as the electron-extraction layer of OPDs. In addition, the good on/off ratio can be maintained in a wide concentration range of 2,2′-(1,3-phenylene)bis[5-(4-tert-butylphenyl)-1,3,4-oxadiazole] (OXD-7) from 25% to 3.75% in the *N,N′*-bis(naphthalen-1-yl)-*N,N′*-bis(phenyl)benzidine (NPB):OXD-7 active layer and the corresponding OPDs can also achieve a fast response time simultaneously, good for its practical application. With the optimized device structure, a large detectivity of over 10^{12} Jones covering the UV-A region (320–400 nm) and a high linear dynamic range of 100 dB are obtained. Additionally, stability of TiO_2-based OPDs, which is not well studied but an important parameter for OPDs, is experimentally investigated.

1. Introduction

Ultraviolet (UV) photodetectors (PDs) have drawn wide interest in the past decades due to broad applications in scientific, industrial, medical, and astronomical fields.[1–6] These practical uses, including biological/chemical sensing, ozone detection, smoke/fire monitoring, and missile warning, require that UV PDs exhibit high on/off ratio (i.e., photocurrent over dark current), fast response time, and a long lifetime, etc.[2,4,6] Previously, much efforts have been paid to fabricate inorganic UV PDs, such as gallium nitride, diamond, and aluminum gallium nitride, etc.[7] Although excellent performance has been achieved by these inorganic devices, expensive substrates, challenges of growing high-quality large-bandgap p/n type semiconductors (bandgap > 3.0 eV), complicated fabricated methods, and requirements of substrates will impede their further development in low-cost, large-area, and flexible UV detection devices.[8] Recently, solution-process inorganic semiconductor nanoparticles have been adopted to fabricate light-detection devices, which demonstrate ultrahigh photocurrent gain, nonetheless, these devices are accompanied by high operation voltage, low on/off ratio, and slow response time.[9]

Different from conventional inorganic UV PDs, UV PDs utilizing organic semiconductors with flexible bandgap engineering, less restricted substrates, and simple fabrication offer a promising pathway for low-cost, large-area, and flexible UV PDs.[10] The majority of previously reported UV organic PDs (OPDs) achieved high efficiency comparable with inorganic counterparts. Although some OPDs had external quantum efficiency (EQE) over unity, a large dark current density was obtained simultaneously. Hence, low on/off ratio near or less than 10^3 was observed when these OPDs were operated at a monochromatic light with the wavelength of 365 nm and intensity of about 1 mW.cm^{-2}.[4,11–13] For example, hybrid planar-bulk-heterojunction UV OPDs consisted of 4,4′,4″-tri-(2-methylphenyl phenylamino) triphenylaine (m-MTDATA)/m-MTDATA:aluminum (III) bis(2-methyl-8-quinolinato)4-phenylphenolate (BAlq)/BAlq were demonstrated with a high EQE of 175% at a reverse voltage of 7 V, whereas the on/off ratio was approximately 1.9×10^3 when the intensity of 365 nm incident light was about 1.2 mW.cm^{-2}.[11] Bilayer UV OPDs of poly(9,9-dihexylfluorene-2,2-diyl) (PFH)/a silane-containing triazine derivative (NSN) with a high responsivity of 0.696 A/W (corresponding EQE is 236.5%) at a large voltage of –12 V were reported that the on/off ratio was about 5×10^2 when the devices were illuminated by a monochromatic light of 365 nm with an intensity of 1 mW.cm^{-2}.[13] These high-efficiency UV OPDs are operated at a large reverse voltage, which can effectively increase electric field within OPDs, reduce the probability of excitons recombination and raise the efficiency of excitons dissociation, thereby boosting EQE.[14,15] Nevertheless, large dark current due to the large reverse bias will also be obtained. Electron/hole blocking layers have been proposed to suppress dark current in OPDs and nanocrystal infrared PDs, dark current still remained 10^{-6} to 10^{-7} A/cm^2 when these devices were operated at a large reverse bias.[16]

Up to now, photovoltaic mode (i.e., self-powered or zero-bias operation mode) PDs were mainly reported in inorganic PDs,[15,17] but not systematically investigated in UV OPDs. Without the need of external driving circuit, photovoltaic mode

H. L. Zhu, Prof. W. C. H. Choy, Dr. W. E. I. Sha, X. Ren
Department of Electrical and Electronic Engineering
The University of Hong Kong
Pokfulam Road, Hong Kong, China
E-mail: chchoy@eee.hku.hk

DOI: 10.1002/adom.201400227

OPDs can reduce the cost and most importantly achieve dark current at a minimum. However, small photocurrent response may be achieved due to the weak electric field compared with those devices worked under a large reverse bias. Hence, one of the challenges for photovoltaic mode UV OPDs is to raise photocurrent response, thereby increasing the on/off ratio. Furthermore, to achieve the high on/off ratio, we conceived a tunable concept of contact impedance. A good contact should satisfy the following conditions in PDs: (1) under dark current condition, carrier-extraction layer-metal interface forms high-impedance contact or Schottky contact to block charges injection into the device; and (2) under light illumination, the interface forms low-impedance contact or Ohmic contact to facilitate the collection of photogenerated carriers at electrodes. With this consideration, we introduce TiO_2 material into our structures to realize these requirements. Most importantly, the tunable contact impedance concept could be extended to other light-sensitive carrier-extraction materials.

In this work, through exploring ultrafast response of trap filling process (<500 ps)[18] and reduction of effective carrier transport barrier induced by UV-activated TiO_2 nanocrystal electron-extraction layer, we proposed and demonstrated excellent repeatable UV OPDs operated at the photovoltaic mode. A high on/off ratio of over 10^5 under the illumination of 350 nm monochromatic light at an intensity of 1 $mW.cm^{-2}$ and a fast rise time of 20 ns (a decay time of 888 ns) are successfully demonstrated. Long-term stability (photocurrent and on/off ratio versus operated time) has also been investigated. For the device structures, our results show that the maximum on/off ratio can be maintained when the concentration of 2,2′-(1,3-Phenylene)bis[5-(4-tert-butylphenyl)-1,3,4-oxadiazole] (OXD-7) in the mixed N,N′-bis(naphthalen-1-yl)-N,N′-bis(phenyl)benzidine (NPB):OXD-7 active layer changes from 25% to 3.75%, and the corresponding OPDs can also achieve fast response time simultaneously. Consequently, the OPDs with high on/off ratio and fast response time can be easily realized for practical applications.

2. Results and Discussions

2.1. Device Structure and Optimization

NPB and OXD-7 are utilized as the electron donor and acceptor, respectively. Their corresponding molecular structures are shown in **Figure 1**(a). NPB has been successfully adopted as the electron donor in previously reported OPDs.[19] Although acceptor OXD-7 has been widely utilized as the electron-transport layer in organic light-emitting diodes,[20] its excellent electrical property and the strong UV absorption, which may be beneficial for UV detection, has not introduced to UV OPDs yet. In our proposed OPDs, the optimized device structure is indium tin oxide (ITO)/TiO_2 (~20 nm)/NPB:OXD-7 (40 nm and the OXD-7 concentration of 12.5%)/MoO_3 (6 nm)/Al (120 nm), as shown in Figure 1(b). The absorbance spectra of thin films of pristine NPB, OXD-7, and the bulk NPB:OXD-7 are shown in Figure 1(c). The bulk NPB:OXD-7 film reveals a absorption superposition of pristine NPB and OXD-7 film, indicating no ground state charge-transfer interaction[21] between donor NPB and acceptor OXD-7. Interestingly, the bulk film achieves

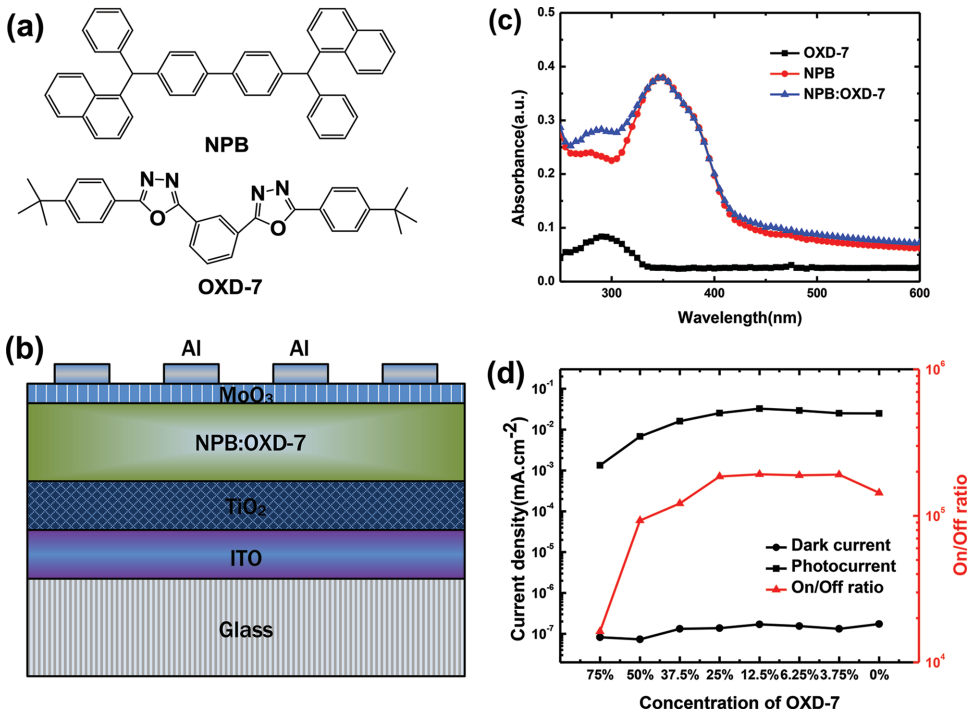

Figure 1. a) Molecular structures of donor NPB and acceptor OXD-7. b) Schematic diagram of device structure consisted of glass/ITO/TiO_2/NPB:OXD-7/MoO_3/Al. c) Absorbance spectra of thin films of pristine NPB, OXD-7, and bulk NPB:OXD-7. Thin films are evaporated on the clean quartz substrates. d) Performance (dark current, photocurrent and on/off ratio) versus various concentrations of OXD-7 acceptor in the active layer.

a strong absorption in the UV range, which is very useful for UV detectors. It should be noted that in the discussion below, unless specify, the testing light source for studying the OPDs is the monochromatic light with the wavelength of 350 nm and intensity of 1 mW.cm^{-2}.

In optimizing our devices, the concentration of OXD-7 acceptor in the active layer, the thickness of active layer and the thickness of TiO_2 layer have been investigated. The larger photocurrent density has been achieved by reducing OXD-7 concentration in the active layer, as shown in Figure 1(d), originating from the increased absorption of the bulk film in the UV-A (320–400 nm) region (See Supporting Information Figure S1). Remarkably, OPDs can achieve maximum on/off ratio in a wide concentration range of OXD-7 from 25% to 3.75%. It is because the photocurrent density maintains at its highest values when OXD-7 concentration is less than 25% and the dark current density is at its lowest value simultaneously. Consequently, there is a large window of OXD-7 concentration to make high performance OPDs (i.e., robust for practical applications). In addition, these OPDs can achieve fast response time simultaneously as described in Section 2.2.

Regarding the thickness of active layer (See Supporting Information Figure S2), photocurrent density and on/off ratio reach the highest value at the thickness of 40 nm. Concerning the effects of TiO_2 (See Supporting Information Figure S3), the best performance can be achieved at the 20 nm thick TiO_2, thicker TiO_2 with imperfect lattice will reduce photocurrent response and increase dark current density.[22] Consequently, the architecture of our devices is optimized as ITO/TiO_2 (~20 nm)/NPB:OXD-7 (40 nm and the OXD-7 concentration of 12.5%)/MoO_3/Al.

2.2. Device Performance

We firstly investigate the current density versus applied voltage measured in the dark and under the UV illumination. For the case without TiO_2 electron-extraction layer, OPDs have no obvious p-n junction characteristics (See Supporting Information Figure S4) and the on/off ratio of near 10^4 at the photovoltaic mode is obtained. Differently, by incorporating the TiO_2 electron-extraction layer, a clear dark current rectification ratio of approximately 10 at ±1 V is achieved as shown in **Figure 2**(a). There is a manifest different feature between photocurrent and dark current and the on/off ratio of 1.6×10^5 at the photovoltaic mode is achieved due to the fact that the photocurrent harvested from TiO_2 based OPDs is more than one order of magnitude larger than that of the OPDs without TiO_2 electron-extraction layer (See Supporting Information Figure S4). By applying a reverse bias to the TiO_2 based OPDs, dark current increases dramatically. For instance, at reverse bias of 1 V, dark current density shoots up three orders of magnitude (as compared to that of the photovoltaic mode), while photocurrent grows less than one order of magnitude. Therefore, the value of on/off ratio is only 7×10^2 at a voltage of −1 V. Consequently, after the introduction of TiO_2 electron-extraction layer, the UV OPDs with the on/off ratio as high as 10^5 at the photovoltaic mode has been achieved.

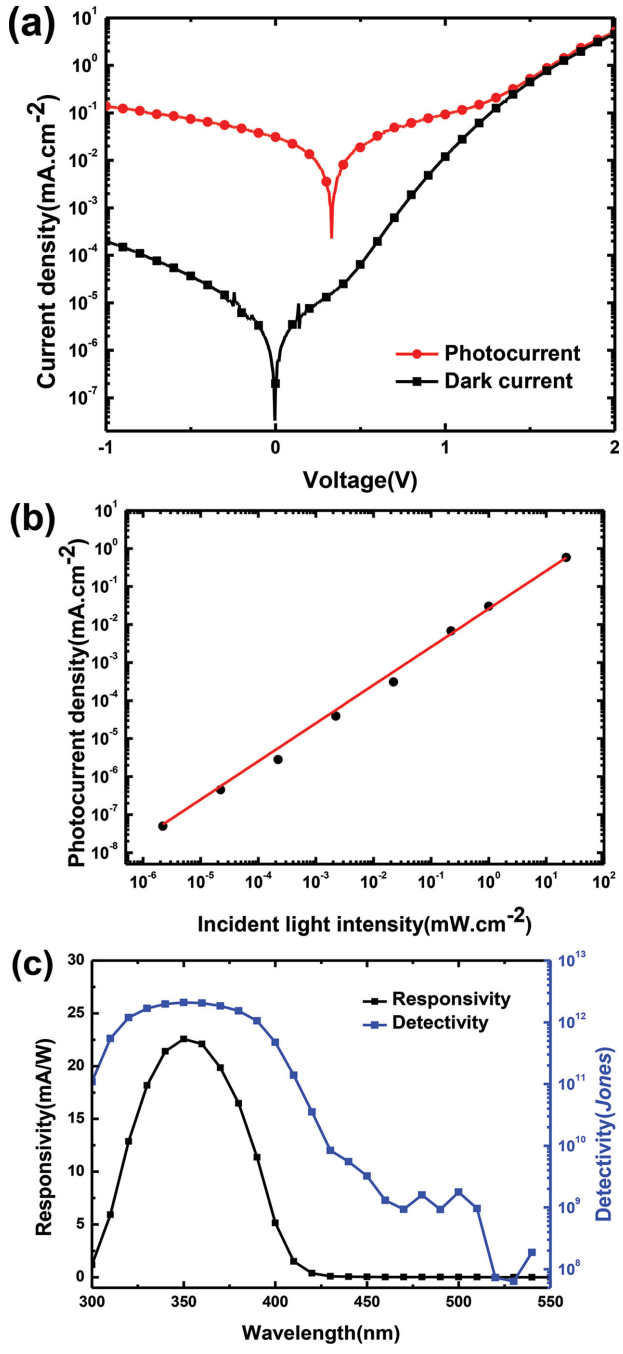

Figure 2. a) Current density-voltage curves of NPB:OXD-7 bulk heterojunction OPDs are obtained at dark room and under the testing light, respectively. b) Linear photocurrent response plot as a function of incident light intensity at the photovoltaic mode. The solid circle stands for experimental data, corresponding fit line is present as well. c) The spectra of responsivity and detectivity versus different wavelength at the photovoltaic mode, where responsivity is calculated by the photocurrent density over incident light intensity, detectivity is determined according to the thermal noise as the dominant noise as detailed in Supporting Information.

The on/off ratio at a given illumination intensity can be examined to compare different PDs sensitivities.[3] In this work, the high on/off ratio of 10^5 is two orders of magnitude larger

than previously reported UV OPDs operated at a large reverse bias,[4,11–13,23] and emerging inorganic nanostructured UV PDs.[15,24] The physical origin of such high on/off ratio of TiO_2 based OPDs will be discussed in the next section in detail.

One important parameter of PDs is the linear dynamic range (LDR) (typically quoted in dB), which can be expressed by $LDR = 20\log(J_{ph}/J_{dark})(dB)$, where J_{ph} is the photocurrent density, measured at the incident light intensity of 1 mW.cm^{-2}, and J_{dark} is the dark current density. When OPDs are operated at the photovoltaic mode, the LDR reaches 100 dB, which is the highest value in UV OPDs, and among the highest reported LDR for inorganic PDs.[5,25] Figure 2(b) shows the photocurrent density as a function of various incident light intensity of 350 nm monochromatic light. Photocurrent density J_{ph} and incident light intensity P_{light} satisfy the relationship $J_{ph} \propto P_{light}^{\alpha}$. By fitting the experimental data, $\alpha = 1.003$ is obtained for our OPDs. The linear response of photocurrent versus the incident light intensity (i.e., α close to 1) suggests that the absence of bimolecular recombination and space-limited charges[26] are achieved in our OPDs.

The *responsivity*, the ratio of photocurrent density to incident light intensity of UV OPDs operated at the photovoltaic mode, is presented in Figure 2(c). The peak responsivity of 22.6 mA/W is obtained at the wavelength of 350 nm, which is consistent with the maximum absorption peak of the bulk NPB:OXD-7 active layer as shown in Figure 1(c). Without TiO_2 layer, the peak responsivity at the photovoltaic mode is only 2 mA/W (See Supporting Information Figure S4), suggesting that TiO_2 layer can effectively improve the efficiency of electrons extraction to electrodes. Meanwhile, the *detectivity* of OPDs at the photovoltaic mode (thermal noise makes a major contribution to the noise current) is shown in Figure 2(c). The optimized OPD reveals a high detectivity with a value of 10^{12} Jones in the UV-A range (320–400 nm), which is also among the highest value in reported UV OPDs.[6,11,27]

Another important parameter of UV OPDs is their photocurrent response time, which has been scarcely investigated in previous UV OPDs.[6] By using a 355 nm picosecond pulse laser, the transient photocurrent response of our OPDs was measured. As shown in **Figure 3**, at the photovoltaic mode, a rise time (defined as photocurrent reaching from 10% to 90% of the maximum photocurrent) of 20 ns and a decay time (defined as photocurrent reducing from 90% to 10% of the maximum photocurrent) of 888 ns are achieved. The response time is three orders of magnitude faster than previously reported UV OPDs.[6,28] Noticeably, the rise time is shorter than the corresponding decay time, which will influence empirical applications. This large decay time can be reduced to 380 ns when the thickness of active layer raises to 140 nm, as shown in Figure S5. Such fast response time makes our UV OPDs suitable for promising applications in missile warning, biological/chemical sensing, smoke/fire monitoring, and high-speed UV imaging. It should be mentioned that rise time and decay time are a function of the intensity of incident light. From our results, both the rise time and decay time fall with increasing the intensity of indicent light, and then tend to saturate at the high light intensity, as shown in Figure S6. This reduction of rise time and decay time with increasing intensity of incident light could be ascribed to varying-concentration-distribution induced traps in the bandgap.[29] Meanwhile, it is interesting to note that the OPDs which maintain the maximum on/off ratio in a wide OXD-7 concentration range (from 25% to 3.75%) as described in Section 2.1, can also achieve fast response time shown in Figure S7 simultaneously, which might be attributed to little mobility change in low OXD-7 concentration doped NPB. Thus, it is desirable for practical applications to obtain high on/off ratio and fast response time simultaneously under the low requirement of OXD-7 concentration.

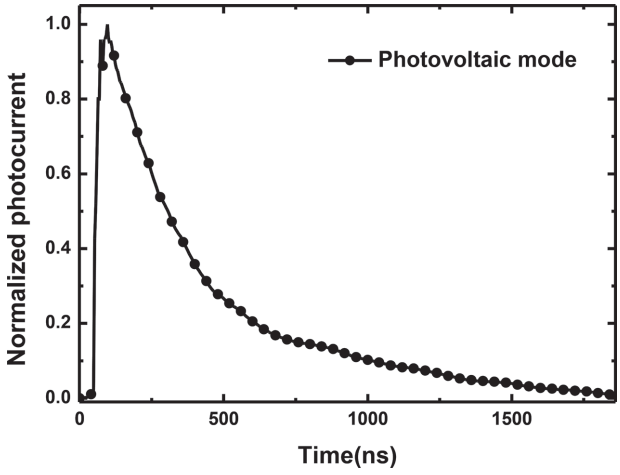

Figure 3. Transient photocurrent response of OPDs operated at the photovoltaic mode.

Stability is of importance for the practical applications of UV OPDs. However, this issue has not commonly studied to date in the most of the reported UV OPDs.[13,19,23,25,27,28,30] One report stated that UV OPDs with m-MTDATA donor could keep 67% of the maximum photocurrent after continuous UV illumination up to roughly 1000 minutes.[11] Very recently, the bulk film of organic layers in UV OPDs has presented no detectable changes in photophysical features under prolonged UV irradiation, indicating the possibility of realizing UV OPDs with the long stability.[31] The testing light was used to illuminate continuously on NPB:OXD-7 based OPDs to study the stability of photocurrent and on/off ratio, shown in **Figure 4**. The photocurrent of our OPDs increases gradually to its peak after an initial stage of illumination. The underlying physics will be discussed in the next section. After that, the photocurrent maintains stably at its peak value with less than 5% drop after continuous illumination up to roughly 660 min, indicating the excellent stability of NPB:OXD-7 based UV OPDs. The prolonged stability of our UV OPDs, compared with m-MTDATA based devices, should be ascribed to two reasons. One reason is that the hole-transport material NPB is more UV-stable than m-MTDATA.[31] The other reason is that the direct contact between organic semiconductors and electrodes will degrade the stability of m-MTDATA based OPDs.[31,32] In our UV OPDs, firstly NPB donor is UV stable. Secondly, the use of interface layers of TiO_2 and MoO_3 contributes to not only improving contact extraction but also avoiding the direct contact of NPB:OXD-7 and electrodes. Consequently, apart from improving the electrical properties, the insertion of interface layers (TiO_2 and MoO_3) also ensure the stability of our UV OPDs.

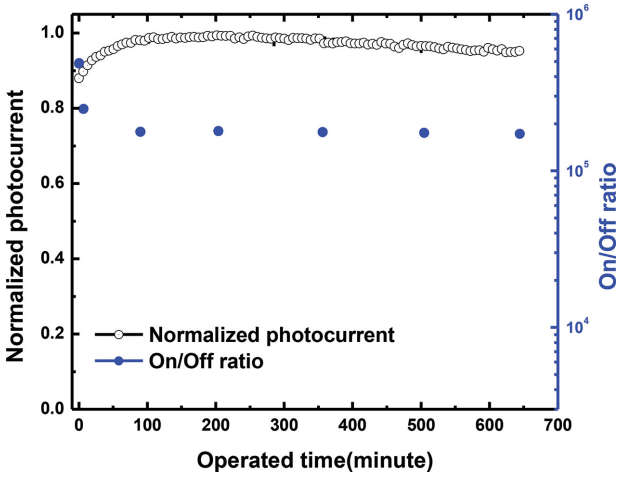

Figure 4. The plot of normalized photocurrent (open circles) and on/off ratio (solid circles) versus continuous operated time.

At the same time, as shown in Figure 4, the on/off ratio reaches a large value of 4.8×10^5 at the very beginning. After the illumination of the testing light, the on/off ratio stabilizes 1.7×10^5. The higher on/off ratio at the beginning is due to the ultralow dark current density of 5.48×10^{-11} A.cm^{-2}. After reaching the saturation stage, although the dark current density increases to 1.66×10^{-10} A.cm^{-2}, the value is still three orders of magnitude lower than previously reported UV OPDs.[11–13,23,27] With the very stable and enhanced photocurrent as shown in Figure 4, the stable on/off ratio of 1.7×10^5 has been achieved.

2.3. Understanding the Effects of the TiO_2 Layer and Working Principles of Devices

To understand the high on/off ratio of TiO_2 based OPDs, we not only experimentally study the work function change of TiO_2 layer due to UV irradiation but also theoretically investigate the electrical properties by rigorously solving the Maxwell's equations and organic semiconductor equations.[33] Generally, there are trap states in unactivated TiO_2, which will lead into an effective extraction barrier between the active layer and TiO_2 and the effective injection barrier between TiO_2 and electrode (high-impedance contact).[34,35] After UV irradiation, trap filling is realized by electrons generated in TiO_2 layer, which would effectively lower the barriers (low-impedance contact). As shown in Figure S8, the work function of TiO_2 layer gradually reduces under UV irradiation, indicating the graduate increase of carrier density within TiO_2 layer (induced by trap filling), which can explain the gradually increased photocurrent when our OPDs were UV irradiated at the very beginning, shown in Figure 4. As a result, the conductivity of TiO_2 will increase under continuous UV illumination and tend to be saturated.[34] Therefore, in our theoretical model, high barriers (0.5 eV) are employed to simulate trap states of unactivated TiO_2 layer, while low barriers of 0.2 eV are used to describe the state of UV-activated TiO_2. The distribution of electron density with respect to two different barriers is shown in **Figure 5**(a). For unactivated TiO_2 incorporated devices, due to the large barriers,

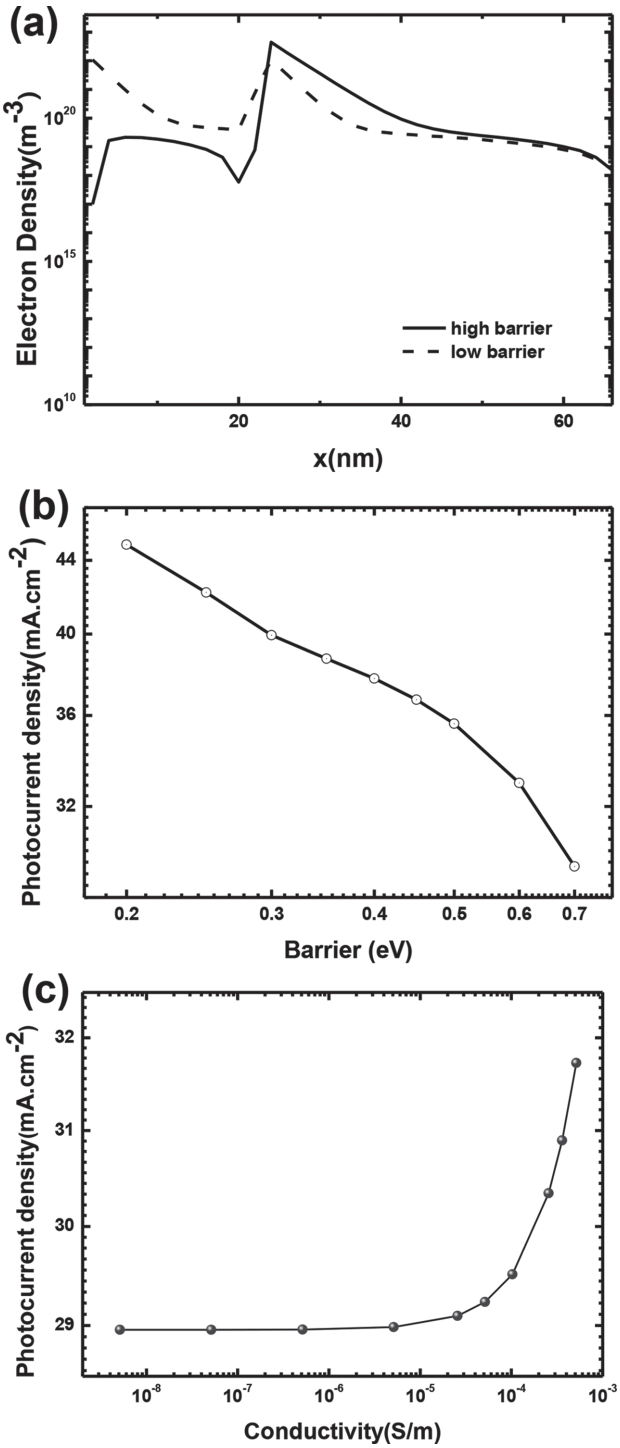

Figure 5. a) The distribution of electron density of the UV OPDs at high and low barrier heights, respectively. The device architecture is cathode/TiO_2 (20 nm)/active layer (40 nm)/MoO_3 (6 nm)/anode. Cathode is located at x = 0. b) Photocurrent density obtained at the photovoltaic mode as a function of various barriers. c) Photocurrent density obtained at the photovoltaic mode as a function of various conductivity of TiO_2.

electrons cannot transport effectively through the TiO_2 layer (i.e., low dark current). However, for OPDs with UV-activated TiO_2 layer due to the effectively low barriers, photocurrent can

be easily extracted to the electrode. The photocurrent as a function of the barrier height is presented in Figure 5(b). The significant increase of photocurrent can be observed with reduced barrier height. Most importantly, due to the unsaturated trap filling by electron leakage from TiO_2 to cathode, the barrier height will go up and down respectively when the UV light is off and on, which increases the on/off ratio to a great extent. In addition, the photocurrent enhancement is also related to the improved conductivity of UV-activated TiO_2, as shown in Figure 5(c). Similarly, as UV light turns on and off repeatedly, the oscillating electron density in the TiO_2 layer induces oscillating conductivity with alternatively low and high series resistances. This also enhances the on/off ratio of OPDs. This light-induced tuning of barrier height and series resistances is clearly observed in different work function responses of TiO_2 with/without UV-activation, shown in Figure S8. Consequently, the physical origin of the large on/off ratio lies at light-induced tuning of barrier height between TiO_2 and active layer and light-induced tuning of series resistance of TiO_2 layer.

Apart from studying the light-induced tuning of barrier heights and series resistance on the on/off ratio of OPDs, we also explore ultrafast response feature of trap filling process tailoring to fast response time requirement for OPDs. This ultrafast response feature has been strongly confirmed by femtosecond transient absorption spectroscopy.[18] At the generation process, immediately after photo-excitation (~200 fs), some of generated free electrons are trapped at surface sites and the rest are trapped in the bulk. Electrons will migrate between surface trap sites and shallow bulk trap sites, which are in equilibrium. At the relaxation processes, shallow trapped electrons relax into deeper sites with a time constant of 500 ps through a hopping process. As the occupation of deep trapping sites increases, the proportion of shallow trapped carriers becomes dominant, resulting in an enhanced mobile charge carriers and their mobility.[36] This effect is known as trap filling. In sum, the total time scale of generation and relaxation processes, i.e., response time of trap filling process, is smaller than 1 ns, which enables a fast response speed of OPDs.

With the study of the effects of TiO_2 layer, we can understand the working mechanism of the OPDs as shown in **Figure 6**. Under dark room condition (see Figure 6(a)), an effective extraction barrier between the active layer and TiO_2 as well as the effective injection barrier between TiO_2 and electrode induced by trap states in unactivated TiO_2 will form high-impedance contact at carrier-extraction layer-metal interface, which impedes charges injection into the device[37] and thus very low dark current can be obtained. After UV radiation, part of photogenerated free electrons are trapped at surface sites and the rest are trapped in the bulk.[18] Since these two species of trap states are energetically equivalent and probably very close to the conduction band edge, electrons are capable of migrating between surface trap sites and shallow bulk trap sites when are in equilibrium stage.[18] At the relaxation processes, shallow bulk trapped electrons relax into deeper bulk sites through a hopping process (see Figure 6(b)). As the occupation of deep trapping sites increases, the proportion of shallow trapped carriers becomes dominant, resulting in an increased mobile charge carriers and their mobility.[36,38] The increased mobile charge carriers will make the Fermi level rise up and reduce the work function of TiO_2. Meanwhile, the increased conductivity induced by increased mobile charge carriers and their mobility and reduced work function will lower the effective barriers at the TiO_2 interfaces. Hence, after UV photo-excitation, carrier-extraction layer-metal interface forms low-impedance contact to facilitate the collection of photogenerated carriers at electrodes (see Figure 6(c)).

3. Conclusion

We have developed a photovoltaic mode UV OPD, utilizing the bulk heterojunction consisting of an NPB donor and OXD-7 acceptor. Incorporating the electron-extraction layer of TiO_2, our devices can achieve a repeatable on/off ratio of 10^5, a large detectivity of over 10^{12} jones covering the UV-A region (320–400 nm), and a high LDR of 100 dB. A fast rise time of 20 ns and a decay time of 888 ns were demonstrated for our OPDs without external bias. The OPDs can achieve this good on/off ratio and response time for a wide concentration range of OXD-7 from 25% to 3.75% in the NPB:OXD-7 active layer

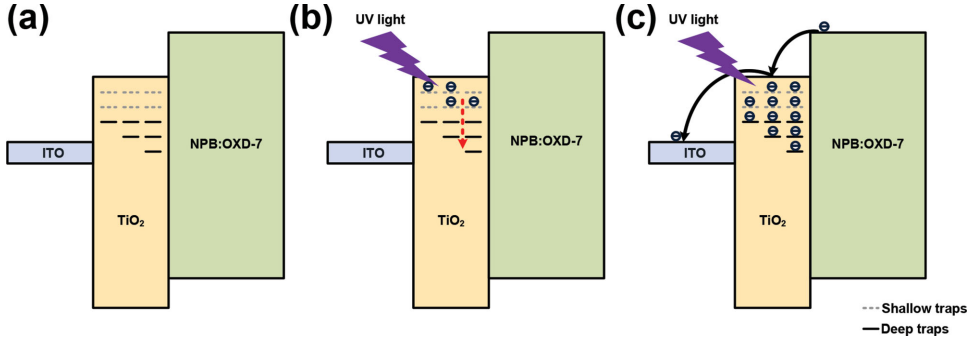

Figure 6. Schematic diagram showing the working mechanism of the OPDs. a) Under dark room condition, trap states in bulk TiO_2 film induce high-impedance contact to block charges injection into the device. b) After UV photo-excitation (~200 fs), some photogenerated free electrons are trapped at surface sites and the rest are trapped in the bulk. Shallow bulk trapped electrons relax into deeper bulk sites with a time constant of 500 ps through a hopping process,[18] shown as the red down arrow. c) As the occupation of deep trapping sites increases, the proportion of shallow trapped carriers becomes dominant, resulting in an increased mobile charge carriers and their mobility.[36,38] Consequently, after UV photo-excitation, reduced work function and increased conductivity of TiO_2 film will induce low-impedance contact at carrier-extraction layer-metal interface, which facilitate the collection of photogenerated carriers at electrodes.

(i.e., robust for device fabrication). The long-term stability (photocurrent and on/off ratio versus operated time) is carefully investigated: photocurrent firstly increases moderately to its peak and then maintains its peak value with less than a 5% drop after continuous illumination up to several hours. As a result, the on/off ratio stabilizes at 1.7×10^5. The experimental and theoretical studies show that such a high on/off ratio results from light-induced tuning of the injection and extraction barriers as well as series resistance of the TiO_2 layer. Consequently, our results show that TiO_2-based NPB:OXD-7 UV OPDs can offer a promising alternative to fabricate stable UV-detection devices and for high-speed UV imaging.

4. Experimental Section

Synthesis and Device Fabrication: Anatase phase TiO_2 nanocrystals were synthesized by a non-aqueous method described elsewhere,[39] and well-synthesize nanocrystals were dissolved in ethanol. The UV OPDs were fabricated on the clean conductive ITO coated glass substrates (square resistance of ~20 Ω/sq.), which were previously cleaned in ultrasonic bath in detergent, deionized water, acetone, ethanol, subsequently. After dried by nitrogen gas, substrates were processed by UV-Ozone treatment for 10 min. The electron-extraction layer TiO_2 of ~20 nm was spin-coated and annealed at 150 °C for 10 min in ambient atmosphere. For thicker TiO_2, spin-coating original TiO_2 solution layer and layer was employed. After that, a blend NPB:OXD-7 layer was deposited by thermal evaporation at the evaporation rate of 0.04 nm/sec. MoO_3 (6 nm) and Al cathode (120 nm) were evaporated in sequence onto the organic active layer to complete the UV OPDs. The evaporation rate and the final thickness of the active layer were controlled by in situ quartz monitors. The film thickness of TiO_2 was measured with AMBIOS XP-2 stylus profilometer. The OPDs were encapsulated in nitrogen-filled glove box. All of the materials we utilized in this work were commercially available and used without further purification.

Device Characterization: The optical transmittance of pristine NPB, OXD-7 and bulk NPB:OXD-7 film was measured by ellipsometer. Absorbance spectrum was determined from the optical transmittance.

Current density as a function of operated voltage (J–V curves) and of different wavelength (responsivity) was measured by combining Keithley 2635 source meter and a light source setup of 1000 W Xenon Arc lamp integrated with a monochromator. The intensity of monochromatic light was measured by facility calibrated (Newport) Si photodetectors. Detectivity was calculated according to thermal noise at the photovoltaic mode as the dominant noise. Dynamic range measurement was performed by changing different intensity of monochromatic light using various neutral filters. The transient photocurrent measurement by using a 355 nm picosecond-pulse laser integrated with an optical chopper and a high speed oscilloscope. Different work function of TiO_2 electron-extraction layer with/without UV-activation was measured by the Kelvin probe system and the 365 nm LED with the intensity of ~1 $mW.cm^{-2}$ was utilized as the excited light sources. All the measurements were carried out at room temperature in the ambient condition.

Simulation Theory: The multiphysics theoretical model of OPDs is governed by Maxwell's equations and semiconductor equations (Poisson, continuity, and drift-diffusion equations).[33] The unified finite-difference (FD) approach was adopted to model the electrical properties of our OPDs. To consider the effective carrier injection and extraction barriers owing to the insertion of TiO_2 layer, the internal electric fields, which strongly affect the drift current, can be given by

$$E_n = -\nabla\varphi - \frac{\nabla\chi}{e} - \frac{k_B T}{e}\nabla\left[\ln(N_c)\right]$$

$$E_p = -\nabla\varphi - \frac{\nabla\chi}{e} - \frac{\nabla E_g}{e} + \frac{k_B T}{e}\nabla\left[\ln(N_v)\right]$$

where E_n and E_p are internal E-fields for electrons and holes, respectively. χ is the electron affinity and E_g is the band gap. Moreover, N_c and N_v are effective density of states (DOS) for electrons and holes, respectively. The extraction barrier can be formed by the jumping of the electron affinity and effective DOS at the interface between buffer and active layer.

Supporting Information

Supporting Information is available from the Wiley Online Library or from the author.

Acknowledgements

H. L. Zhu and W. C. H. Choy contributed equally to this work. This work is supported by University Grant Council of the University of Hong Kong (grants #10401466 and #201111159062), and the General Research Fund (grants: HKU711813 and HKU711612E), the RGC-NSFC grant (N_HKU709/12) from the Research Grants Council of Hong Kong Special Administrative Region, China. Authors acknowledge Shunmian Lu and Fengxian Xie for the help of synthesizing TiO_2 nanocrystal.

Received: May 13, 2014
Revised: July 27, 2014
Published online: August 13, 2014

[1] a) Y. A. Goldberg, *Semicond. Sci. Tech.* **1999**, *14*, R41; b) P. Peumans, A. Yakimov, S. R. Forrest, *J. Appl. Phys.* **2003**, *93*, 3693.
[2] E. Monroy, F. Omnès, F. Calle, *Semicond. Sci. Tech.* **2003**, *18*, R33.
[3] G. Konstantatos, E. H. Sargent, *Nat. Nanotechnol.* **2010**, *5*, 391.
[4] H. W. Lin, S. Y. Ku, H. C. Su, C. W. Huang, Y. T. Lin, K. T. Wong, C. C. Wu, *Adv. Mater.* **2005**, *17*, 2489.
[5] F. Guo, B. Yang, Y. Yuan, Z. Xiao, Q. Dong, Y. Bi, J. Huang, *Nat Nano* **2012**, *7*, 798.
[6] K.-J. Baeg, M. Binda, D. Natali, M. Caironi, Y.-Y. Noh, *Adv. Mater.* **2013**, *25*, 4267.
[7] a) F. Yan, X. Xin, S. Aslam, Y. Zhao, D. Franz, J. H. Zhao, M. Weiner, *IEEE J. Quantum Elect.* **2004**, *40*, 1315; b) M. A. Khan, J. N. Kuznia, D. T. Olson, J. M. Van Hove, M. Blasingame, L. F. Reitz, *Appl. Phys. Lett.* **1992**, *60*, 2917; c) M. Razeghi, A. Rogalski, *J. Appl. Phys.* **1996**, *79*, 7433.
[8] G. Yu, Y. Cao, G. Srdanov, *Quantum Sensi. Nanophoton. Devices VI* **1999**, *3629*, 349.
[9] a) J. P. Clifford, G. Konstantatos, K. W. Johnston, S. Hoogland, L. Levina, E. H. Sargent, *Nat Nano* **2009**, *4*, 40; b) H.-Y. Chen, K. F. LoMichael, G. Yang, H. G. Monbouquette, Y. Yang, *Nat Nano* **2008**, *3*, 543; c) G. Konstantatos, J. Clifford, L. Levina, E. H. Sargent, *Nat. Photonics* **2007**, *1*, 531; d) Y. Z. Jin, J. P. Wang, B. Q. Sun, J. C. Blakesley, N. C. Greenham, *Nano Lett.* **2008**, *8*, 1649.
[10] S. R. Forrest, *Nature* **2004**, *428*, 911.
[11] S.-h. Wu, W.-l. Li, B. Chu, C. S. Lee, Z.-s. Su, J.-b. Wang, Q.-j. Ren, Z.-z. Hu, Z.-q. Zhang, *Appl. Phys. Lett.* **2010**, *97*, 023306.
[12] S.-h. Wu, W.-l. Li, B. Chu, C. S. Lee, Z.-s. Su, J.-b. Wang, F. Yan, G. Zhang, Z.-z. Hu, Z.-q. Zhang, *Appl. Phys. Lett.* **2010**, *96*, 093302.
[13] H.-g. Li, G. Wu, H.-Z. Chen, M. Wang, *Org. Electron.* **2011**, *12*, 70.
[14] L. Onsager, *J. Chem. Phys.* **1934**, *2*, 599.
[15] S. M. Hatch, J. Briscoe, S. Dunn, *Adv. Mater.* **2013**, *25*, 867.
[16] a) F. Guo, Z. Xiao, J. Huang, *Adv. Optical Mater.* **2013**, *1*, 289; b) G. Sarasqueta, K. R. Choudhury, J. Subbiah, F. So, *Adv. Funct. Mater.* **2011**, *21*, 167.
[17] a) Y.-Q. Bie, Z.-M. Liao, H.-Z. Zhang, G.-R. Li, Y. Ye, Y.-B. Zhou, J. Xu, Z.-X. Qin, L. Dai, D.-P. Yu, *Adv. Mater.* **2011**, *23*, 649;

b) P.-N. Ni, C.-X. Shan, S.-P. Wang, X.-Y. Liu, D.-Z. Shen, *J. Mater. Chem. C* **2013**, *1*, 4445.
[18] Y. Tamaki, A. Furube, M. Murai, K. Hara, R. Katoh, M. Tachiya, *Phys. Chem. Chem. Phys.* **2007**, *9*, 1453.
[19] Q. Dai, X. Q. Zhang, *Opt. Express* **2010**, *18*, 11821.
[20] T. Yasuda, Y. Yamaguchi, D. C. Zou, T. Tsutsui, *Jpn. J. Appl. Phys.* **2002**, *41*, 5626.
[21] J. J. M. Halls, J. Cornil, D. A. dos Santos, R. Silbey, D. H. Hwang, A. B. Holmes, J. L. Brédas, R. H. Friend, *Phys. Rev. B* **1999**, *60*, 5721.
[22] L. Vivien, A. Polzer, D. Marris-Morini, J. Osmond, J. M. Hartmann, P. Crozat, E. Cassan, C. Kopp, H. Zimmermann, J. M. Fédéli, *Opt. Express* **2012**, *20*, 1096.
[23] L. Zhu, W. S. Wang, Z. G. Yao, X. Q. Zhang, Y. S. Wang, *IEEE T. Electron Dev.* **2012**, *59*, 3583.
[24] L. Hu, J. Yan, M. Liao, H. Xiang, X. Gong, L. Zhang, X. Fang, *Adv. Mater.* **2012**, *24*, 2305.
[25] X. Gong, M. Tong, Y. Xia, W. Cai, J. S. Moon, Y. Cao, G. Yu, C.-L. Shieh, B. Nilsson, A. J. Heeger, *Science* **2009**, *325*, 1665.
[26] a) L. J. A. Koster, V. D. Mihailetchi, H. Xie, P. W. M. Blom, *Appl. Phys. Lett.* **2005**, *87*, 203502; b) P. Schilinsky, C. Waldauf, C. J. Brabec, *Appl. Phys. Lett.* **2002**, *81*, 3885.
[27] L. Zhu, Q. Dai, Z. F. Hu, X. Q. Zhang, Y. S. Wang, *Opt. Lett.* **2011**, *36*, 1821.
[28] a) D. Ray, K. L. Narasimhan, *Appl. Phys. Lett.* **2007**, *91*, 093516; b) G. Zhang, W. Li, B. Chu, Z. Su, D. Yang, F. Yan, Y. Chen, D. Zhang, L. Han, J. Wang, H. Liu, G. Che, Z. Zhang, Z. Hu, *Org. Electron.* **2009**, *10*, 352.
[29] Y. Jiang, W. J. Zhang, J. S. Jie, X. M. Meng, X. Fan, S. T. Lee, *Adv. Funct. Mater.* **2007**, *17*, 1795.
[30] a) L. Zhu, W. S. Wang, Z. G. Yao, X. Q. Zhang, Y. S. Wang, *Solid State Electron.* **2013**, *80*, 14; b) Q. Dai, L. Zhu, J. Sun, X. Q. Zhang, Y. S. Wang, *Sci. China Technol. Sci.* **2012**, *55*, 1551; c) L. Zhu, Q. Dai, Z. F. Hu, X. Q. Zhang, Y. S. Wang, *IEEE Photonic. Tech. L.* **2011**, *23*, 1835.
[31] Q. Wang, H. Aziz, *Org. Electron.* **2013**, *14*, 3030.
[32] Q. Wang, G. Williams, T. Tsui, H. Aziz, *J. Appl. Phys.* **2012**, *112*, 064502.
[33] a) W. E. I. Sha, W. C. H. Choy, Y. G. Liu, W. Cho Chew, *Appl. Phys. Lett.* **2011**, *99*, 113304; b) W. E. I. Sha, W. C. H. Choy, W. C. Chew, *Opt. Express* **2010**, *18*, 5993; c) W. E. I. Sha, W. C. H. Choy, Y. Wu, W. C. Chew, *Opt. Express* **2012**, *20*, 2572.
[34] C. S. Kim, S. S. Lee, E. D. Gomez, J. B. Kim, Y.-L. Loo, *Appl. Phys. Lett.* **2009**, *94*, 113302.
[35] a) D. Zhang, W. C. H. Choy, F. Xie, W. E. I. Sha, X. Li, B. Ding, K. Zhang, F. Huang, Y. Cao, *Adv. Funct. Mater.* **2013**, *23*, 4255; b) D. Zhang, W. C. H. Choy, F.-x. Xie, X. Li, *Org. Electron.* **2012**, *13*, 2042.
[36] J. E. Kroeze, T. J. Savenije, J. M. Warman, *J. Am. Chem. Soc.* **2004**, *126*, 7608.
[37] a) V. Duzhko, V. Y. Timoshenko, F. Koch, T. Dittrich, *Phys. Rev. B* **2001**, *64*, 075204; b) S. Sista, M.-H. Park, Z. Hong, Y. Wu, J. Hou, W. L. Kwan, G. Li, Y. Yang, *Adv. Mater.* **2010**, *22*, 380.
[38] a) R. Koenenkamp, R. Henninger, P. Hoyer, *J. Phys. Chem.* **1993**, *97*, 7328; b) J. A. Anta, J. Nelson, N. Quirke, *Phys. Rev. B* **2002**, *65*, 125324.
[39] G. V. Jensen, M. Bremholm, N. Lock, G. R. Deen, T. R. Jensen, B. B. Iversen, M. Niederberger, J. S. Pedersen, H. Birkedal, *Chem. Mater.* **2010**, *22*, 6044.